Materials Research Bulletin 50 (2014) 165–171

Contents lists available at ScienceDirect

Materials Research Bulletin

journal homepage: www.elsevier.com/locate/matresbu

Effects of diethanolamine on sol–gel–processed Cu_2ZnSnS_4 photovoltaic absorber thin films

S. Kahraman *, S. Çetinkaya, H.A. Çetinkara, H.S. Güder

Semiconductor Research Laboratory, Physics Department, Faculty of Art and Science, Mustafa Kemal University, Hatay 31034, Turkey

ARTICLE INFO

Article history:
Received 1 May 2013
Received in revised form 23 September 2013
Accepted 22 October 2013
Available online 30 October 2013

Keywords:
A. chalcogenides
A. semiconductors
A. thin film
B. sol–gel chemistry
C. X-ray diffraction
D. crystal structure

ABSTRACT

As a promising solar absorber, the Cu_2ZnSnS_4 compound has been popular recently for the production of green and economical thin-film solar cells owing to the abundancy and non-toxicity of all the constituents. In this study, we have produced Cu_2ZnSnS_4 films via the sol–gel technique. As a stabilizer, the effects of the diethanolamine on the properties of the films were investigated. The amount of diethanolamine significantly affected the crystal structure, crystallite sizes and phase purity of the films. X-ray diffraction and Raman spectroscopy analyses confirmed the formation of phase-pure CZTS films. It was found that the film produced by using 2 ml of diethanolamine in sol exhibited pure CZTS phase, compact and dense morphology and enhanced photo-sensitivity. Light on/off current ratio of the n-Si/Cu_2ZnSnS_4 junction was found to be 47 under 100 mW/cm^2 of illumination. Electrical activation energies of the films were investigated and the variations were attributed to delocalized phonon states generating from the presence of other phases and lattice defects.

1. Introduction

Extensive use of photovoltaic technologies (PV) has the potential to offer modern society larger long-range economic and environmental sustainability than currently possible with carbon-based fuels. Due to a rapid increase in demand for renewable energy sources, the production of solar cells has increased significantly. In order to make photovoltaic devices more widespread, cheaper, more efficient, greener solar cells have to be developed [1]. To produce PV technologies with capacity of terawatt levels, it is crucial to develop low-cost solar cell materials and technologies.

Thin-film chalcogen materials, especially $CuInSe_2$ (CIS), $CuInGa(S,Se)_2$ (CIGS) and CdTe, are currently used in the production of large-scale, commercial, photovoltaic devices. However, the scarcity of indium and tellurium in the earth's crust limits the future of CIGS- and CdTe-based solar cells. In addition, the price of In and relatedly solar-cell production costs will increase in the near future due to the extensive use of indium in display technologies and opto-electronic devices. Another problem with CdTe-based solar cells is that the cadmium (Cd) is very toxic to health and the environment. This problem has led researchers to search for more abundant and greener materials. Because of its similar properties to the CIGS compound, the I_2-II-IV-VI_4 group has been receiving attention as a new-generation absorber materials. The Cu_2ZnSnS_4 (CZTS) compound is a good candidate for photovoltaic applications as an absorber layer [3–6] and has a direct band gap ranging from 1.4 to 1.6 eV which is close to the optimum value required for a solar cell's absorber layer, a high absorption coefficient in the visible solar spectrum wavelengths and p-type conductivity [7]. However, even though it is a promising absorber material, the studies on CZTS-based solar cells are at an early stage [2]. An efficiency of 11.1% has been reported for CZTS-based solar cells in laboratory conditions [8]. But in view of the fact that the theoretical efficiency of CZTS is about 32.2% [9], more studies are required to increase the efficiency and to develop ecological production methods, which would ensure successful commercialization [10]. CZTS thin films have been prepared via various methods such as physical vapor deposition [2,4,6,11–19], electrochemical deposition [1,20–22], sol–gel [23–32] and successive ionic layer adsorption-reaction methods [33–35,40–42]. Aqueous solution deposition methods have several advantages, very important one being that a variety of thin films can be grown at low temperatures using cheap manufacturing equipment. The sol–gel method is a very simple and low-cost process based on hydrolysis and poly-condensation reactions. Sulfide films can be directly obtained by sulfurizing oxyhydrate precursors. In order to utilize the sol–gel technique for obtaining crack-free, uniform, transparent, and strongly adherent films, sol stabilization is one of the essential steps in the film formation [43]. To stabilize the sol and to reduce the rates of hydrolysis and poly-condensation

* Corresponding author. Tel.: +90 326 2455845/1637; fax: +90 326 2455867.
E-mail addresses: suleymanmku@gmail.com, skahraman@mku.edu.tr (S. Kahraman).

0025-5408/$ – see front matter © 2013 Elsevier Ltd. All rights reserved.
http://dx.doi.org/10.1016/j.materresbull.2013.10.043

reactions by forming complex intermediates [44,45], various stabilization or chelating or complexing agents have been used. Diethanolamine (DEA), diethylenetriamine, monoethanolamine, acetylacetone, acetic acid and polyethylene glycol have widely been used for this purpose [46–52]. Diethanolamine (DEA) is frequently used as a stabilizer in various sol–gel systems [52–55]. To date, several groups have reported CZTS thin films produced via the sol–gel method. However, to the best of our knowledge, the properties of CZTS compound have not been investigated with respect to DEA content. Therefore, in this study we prepared high-quality, dense CZTS thin films on quartz-glass and n-type silicon substrates using the sol–gel spin-coating method and investigated the structural, morphological, electrical and optical properties of CZTS films with respect to DEA content in sol solution. To tolerate sulfur loss during annealing, the annealing process was carried out in a vacuumed quartz tube containing elemental sulfur which is a non-toxic material.

2. Experimental

The CZTS precursor solutions were prepared by dissolving copper (II) acetate monohydrate (0.3 M, 98%), zinc (II) acetate dihydrate (0.3 M, 99.99%), tin (II) cloride (0.3 M, 98%) from Sigma–Aldrich and thiourea (1.2 M, 99.0% from Sigma Aldrich) into 2-methoxyethanol (20 ml, 99.8% from Sigma Aldrich). The final solutions were stirred at 45 °C, 850 rpm for 1 h to dissolve the metal compounds completely. During stirring, 2, 3, 4, and 5 ml of diethanolamine (DEA) were dropped slowly into each solution as a stabilizer. After 24 hours of aging, it was observed that the prepared solutions were stable. The prepared solutions were aged for 24 hours and quartz-glass slides were used as substrates which were ultrasonically cleaned in turn with detergent, nitric acid (1:4), acetone and ethanol for 10 min. To produce the CZTS films, the prepared solutions were spin-coated onto quartz and n-type silicon substrates at 3000 rpm for 30 s followed by solvent-drying at 175 °C for 10 min on a hot plate. The spin-coating and solvent-drying processes were repeated 10 times to obtain the desired thickness of the films. Finally, the samples were subjected to an annealing process for 2 h at 500 °C in a quartz tube containing 10 g of elemental sulfur. Before the annealing, the tube furnace was evacuated to 5×10^{-4} mbar. The heating rate was 5 °C/min. After the annealing process, the samples were allowed to cool naturally to room temperature.

Silver paste was used to obtain ohmic contacts. The structural, morphological and optical properties of the samples were examined by X-ray diffraction (XRD, PANalytical X'Pert PRO MPD with the wavelength of 1.5418 Å Cu Kα radiation), Raman spectroscopy (Confocal Raman spectrometer, Witec alpha 300 with 532 nm light source), scanning electron microscopy (SEM, JEOL JSM 5800), energy dispersive X-ray spectroscopy (EDXS, Oxford Instruments ISIS 300), absorbance spectroscopy (UV/Vis/NIR spectroscopy, Lambda 950 with 150 mm integrating sphere) methods. Resistance-temperature characteristics of the samples were investigated by two point probe method in the temperature range of 300–420 K through a Keithley 6487 interfaced with computer by a Labview program. Photo-transient current of the Ag/n-Si/CZTS/Ag structures were obtained at 2 V under 100 mW/cm^2 of illumination. The intensity of light was measured with a luxmeter (Testo-540).

3. Results and discussions

3.1. Structural studies

CZTS exhibits Kesterite crystal structure with lattice parameters $a = 0.5427$ and $c = 1.0848$ nm [34]. The structural characterization was performed using X-ray diffraction (XRD) and Raman techniques. The diffraction patterns were obtained with a 40 keV operating voltage and a current of 35 mA. The step size and scan step time were 0.0330[?] and 1 s, respectively. Fig. 1 shows the obtained XRD patterns of the films deposited by using the solutions containing different DEA content. The patterns of the films show characteristic peaks (marked with "■"" symbol) of CZTS (JCPDS: 00-026-0575) located at 28.56, 33.07, 47.44 and 56.29[?]. However, the patterns of the samples deposited in the solutions containing 3, 4 and 5 ml DEA show also some other peaks (marked with "*" symbol) indicating the presence of SnS phase (JCPDS: 00-022-0950). From the full width of half maximum (FWHM) analysis [56], mean crystallite size of the films were calculated to be 8, 16, 18, and 21 nm with respect to increasing DEA content (Table 1). As can be seen that mean crystallite sizes of the films significantly increase with increasing DEA content. A similar trend in particle size was obtained from the SEM analysis. As a result it can be concluded that DEA content in the growth solution dramatically affects the crystal structure and phase purity of the CZTS films.

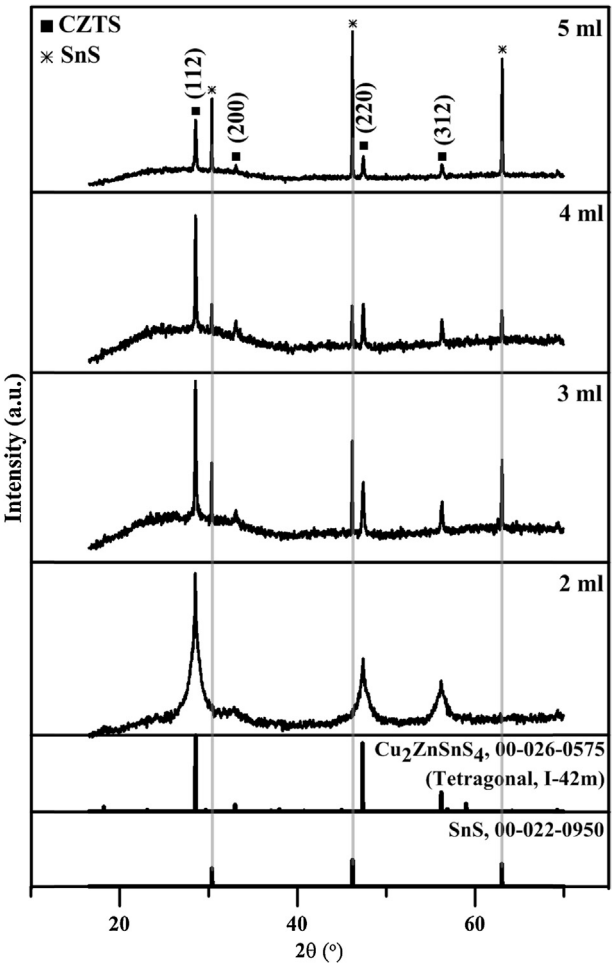

Fig. 1. Obtained XRD patterns of the CZTS films deposited by using the solutions containing different DEA content.

Binary or ternary sulfides such as ZnS, $Cu_{2-x}S$ and Cu_2SnS_3 have similar diffraction patterns to CZTS owing to their similar zinc blend-type structures. To prove the phase purity or to detect the presence of other possible secondary phases, Raman spectroscopy analyses of the samples over the range 200–500 cm^{-1} were also made and the results are given in Fig. 2. In all Raman spectrum of the samples, four obvious peaks at 287, 314, 337, and 371 cm^{-1} can be clearly seen. The peaks seen at 287, 337 and 371 cm^{-1} are in

Table 1
Estimated mean crystallite size, impurity levels' activation energy and optical band gap values of the studied CZTS films.

DEA content	Mean crystallite size (nm)	Impurity levels' electrical activation energies (meV)	Estimated optical band gap value (eV)
2 ml	8	610 200	1.49
3 ml	16	450 195	1.59
4 ml	18	620 215	1.52
5 ml	21	500 210	1.48

good agreement with the reference Raman spectra of CZTS [57] and confirms the formation of the CZTS phase. As detected through XRD studies of the samples which were derived from the solutions containing 3, 4, and 5 ml of DEA, a minor peak at 314 cm^{-1} corresponds to a small amount of SnS_2 phase.

Additionally, the strong major peak at 337 cm^{-1} in all Raman spectrum is an indication of the good crystalline quality of our films. It is note-worthy to mention that the absence of some peaks such as peaks at 351 and 274 cm^{-1} corresponding to ZnS phase, a peak at 475 cm^{-1} corresponding to $Cu_{2-x}S$ and a peak at 345 cm^{-1} corresponding to ZnS:Cu [12,14,58] suggest the absence of these compounds in our CZTS samples.

3.2. Surface morphology

Plane-view SEM images and relative elemental composition results of the semi-quantitative, energy-dispersive X-ray spectroscopy (EDXS) analysis, which just illustrate the elemental composition of the CZTS films, of the CZTS films prepared using different DEA volume in sol solution are shown in Fig. 2. They reveal that all samples show smooth, compact and densely packed morphology and are near to stoichiometry. For the film prepared when the DEA content is 5 ml (Fig. 2a), some cracks and voids were observed through the SEM images. When the DEA concentration was decreased the density of the cracks and voids reduced rapidly (Fig. 2b,c). Finally the cracks and voids disappeared when the DEA concentration was 2 ml in the sol solution (Fig. 2d). Hence, it can be deduced that DEA concentration in the sol is very crucial to

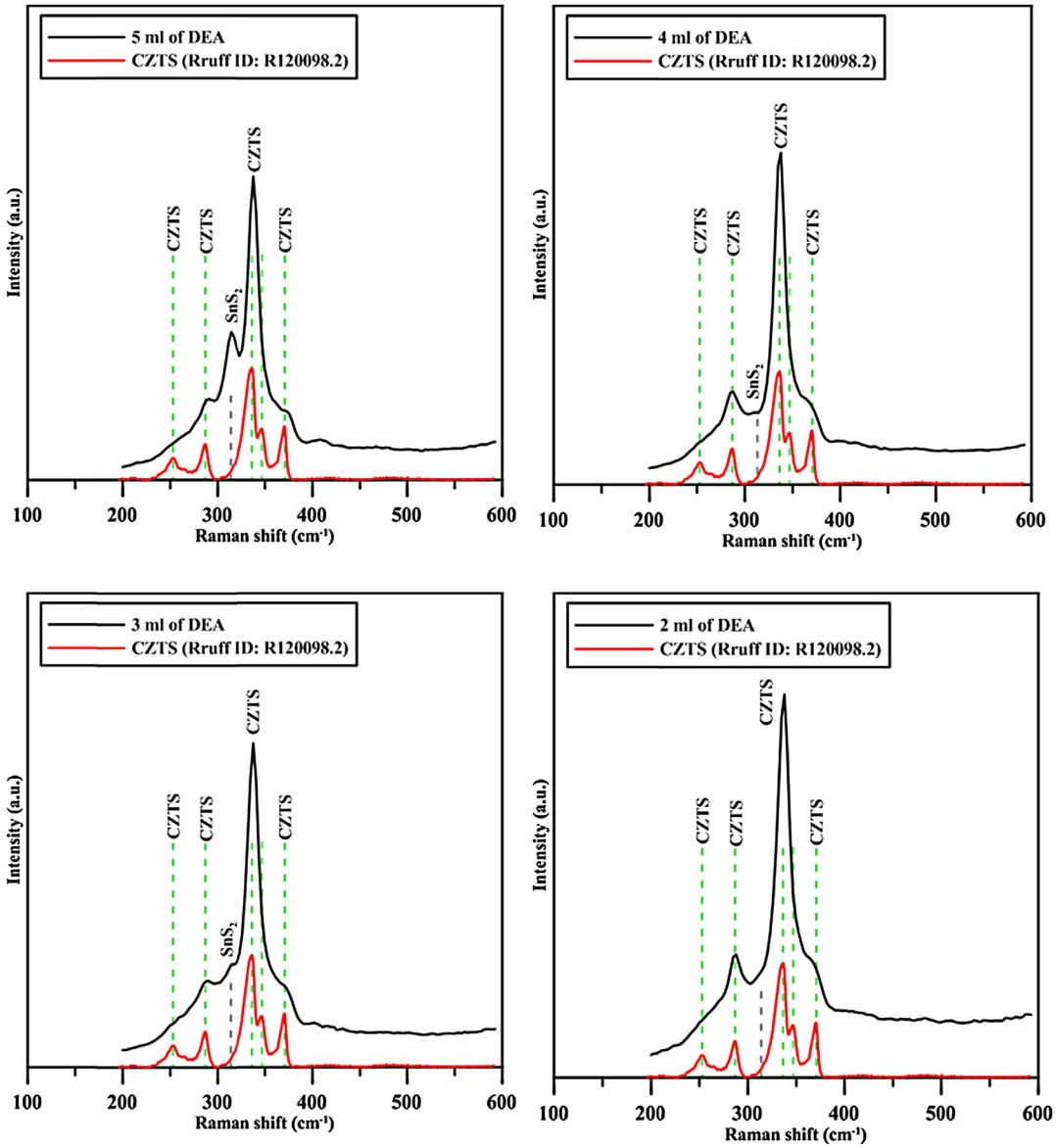

Fig. 2. Raman spectroscopy analyses of the samples.

obtain void/crack-free CZTS thin films. EDXS analysis also show that the samples have excessive sulphur which may be caused by much elemental sulphur used in the sulphurization stage.

3.3. Resistivity-temperature characteristics of the films

In order to find impurity levels' electrical activation energies, resistance-temperature behavior of the samples was investigated in the temperature range of 300–420 K. Silver electrodes were painted on the surface of films to get ohmic contact. It can be concluded from the solid-state theory of semiconductors [33,34], in case of a semiconductor with one or more impurity levels, the temperature dependence of dark electrical resistance is given by

$$R(T) = R_o e^{E_g/2kT} + \sum_{i=1}^{n} R'_{0,i} e^{\Delta E_i/kT} \quad (1)$$

In Eq. (1), $R_o$and $R'_{0,i}$ are constants, E_g is the thermal band gap energy, ΔE_i is the electrical activation energies of the impurity levels, k is Boltzmann constant, and T is temperature. In a relatively lower temperature, the overall conductivity of the semiconductor samples is dominated by the charge carriers generated by ionization of impurity levels (extrinsic conductivity), and thus the second term in Eq. (1) prevails in the R_T dependence. At relatively higher temperatures, besides, the temperature dependence of conductivity is dominated by the band-to-band electronic transitions. The charge carriers acquire enough thermal energy to make an inter-band transition (the intrinsic conductivity is "activated" at these temperatures) under certain conditions [34]. According to previous discussion, the two terms appearing in Eq. (1) may be used independently in the corresponding temperature intervals. So in the graph of ln(R) vs 1000/T, a number of linear trends appear which indicate a number of impurity levels. Thus the second term in Eq. (1) prevails in the R_T dependence in the studied temperature interval (300–420 K). The decrease of dark electrical resistance upon increase of temperature in the region of extrinsic conductivity (corresponding to the lower temperature interval) follows the equation:

$$R(T) = \sum_{i=1}^{n} R'_{0,i} e^{\Delta E_i/kT} \quad (2)$$

Fig. 3 shows ln(R) vs 1000/T graphs of the samples. The presence of two regions with different slops in Fig. 3 suggests that there are two types of conduction mechanism present in the studied samples. By using Eq. (2), ΔE can be easily written as

$$\Delta E = k \frac{d(\ln R(T))}{d(1/T)} \quad (3)$$

Electrical activation energy values of the impurity levels were estimated from the slopes of ln(R) vs 1000/T graphs. The obtained impurity level electrical activation energy (ΔE) values are given in Table 1. These values are in good agreement with the literature [35–39]. The variations in electrical resistivity and activation energies may be related to delocalized phonon states generating from presence of other phases/lattice defects. Disordered networks generate a delocalization of phonons. If the material has more ordered structures, the delocalized phonon states are reduced leading to an improved electrical transport mechanism of the semiconductor material [31].

3.4. Photo-transient current characteristics of the Ag/n-Si/CZTS/Ag structure

To see the potential photo-conversion capability of the CZTS film, an n-Si/CZTS hetero-junction was also fabricated. For this purpose the CZTS precursor solution containing 2 ml of DEA was spin-coated on n-type silicon substrate. The photo-transient

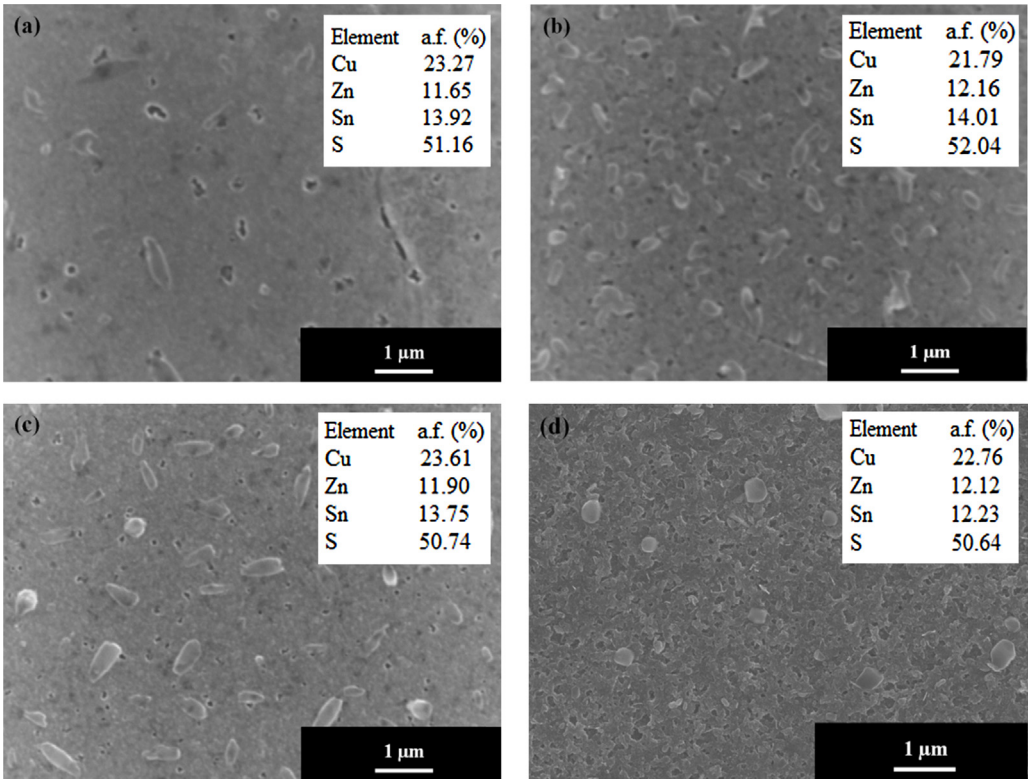

Fig. 3. Plane-view SEM images and relative elemental composition of the CZTS films prepared using different DEA in sol solution a) 5 ml b) 4 ml c) 3 ml d) 2 ml.

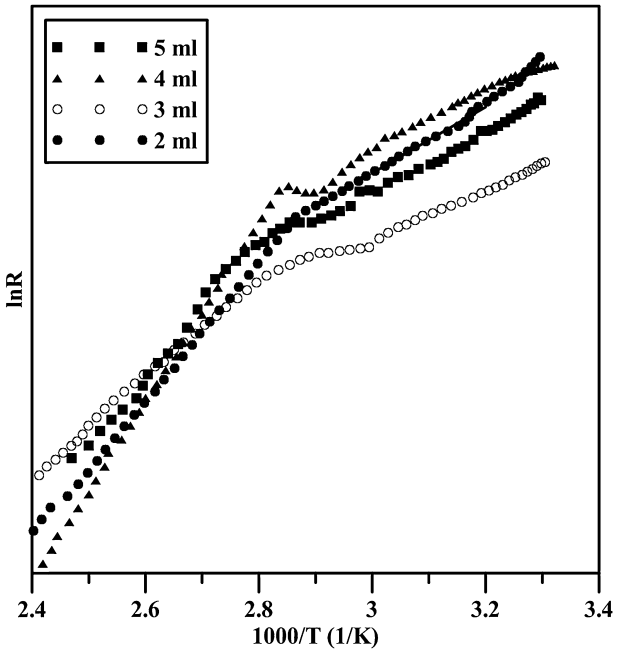

Fig. 4. ln(R) vs 1000/T graphs of the CZTS films.

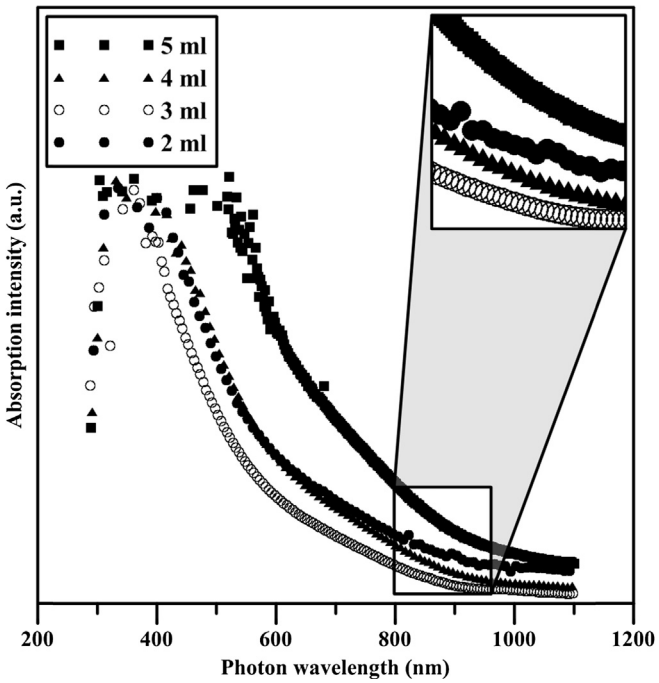

Fig. 6. Optical absorption behavior of the CZTS films.

current curves of the produced Ag/n-Si/CZTS/Ag structure at 2 V under different illuminations are shown in Fig. 4. As seen from the Fig. 4 that the n-Si/CZTS junction exhibits good photo-conductivity and there is a sudden change in the photo-current. The I_{on}/I_{off} ratios for the junction were found to be 47, 35 and 30 for the 100, 75, and 50 mW/cm^2 of illuminations, respectively. This behavior confirms photo-sensitivity of the produced structure and suggests that the I_{on}/I_{off} ratios are enough for solar conversion applications.

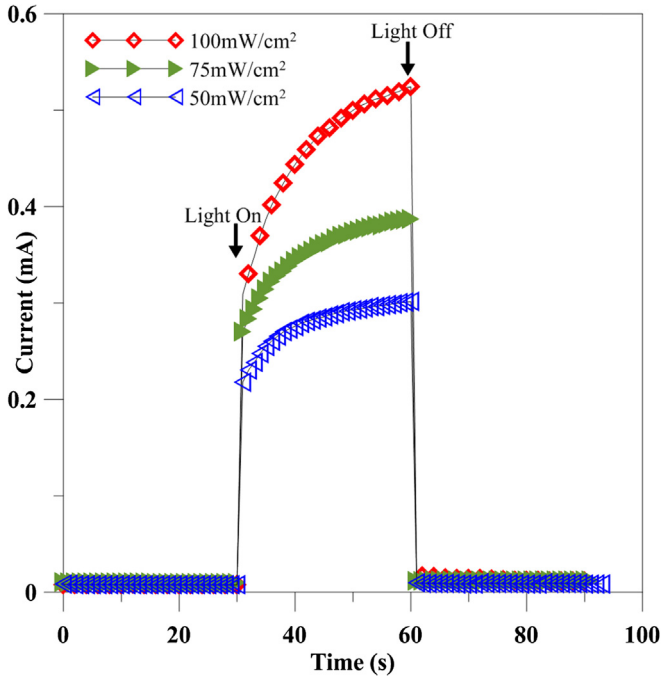

Fig. 5. The photo-transient current curves of the produced Ag/n-Si/CZTS/Ag structure under different illuminations.

3.5. Absorption behavior

Near the absorption edge or in the strong absorption zone of the transmittance spectra, the absorption coefficient is related to the optical energy gap, E_g following the power-law behavior of Tauc's relation [59]

$$(\alpha h\nu) = B(h\nu - E_g)^m \quad (4)$$

Where, B is an energy-independent constant, E_g is the optical band-gap energy and m is an index that characterizes the optical absorption process and is theoretically equal to 2 and 1/2 for the indirect and direct allowed transitions, respectively. Fig. 5 and Fig. 6 show the absorption behavior and the band-gap photon-energy estimations of the CZTS films, respectively. The band-gap estimations were performed by extrapolating the linear region of the plot of $(\alpha h\nu)^2$versus $h\nu$ to the horizontal axis and considering the intersecting point. As can be seen from Fig. 6, the samples exhibit a linear dependence which indicates the directly allowed nature of the films. Thus, we can choose m as 1/2. By plotting the graph of $(\alpha h\nu)^2$against the photon energy$h\nu$, the band gap values were estimated to be 1.49, 1.59, 1.52, and 1.48 eV for the samples deposited in the solutions containing 2, 3, 4, and 5 ml DEA, respectively. The $E_g$value of the CZTS compound, as a p-type direct-band-gap semiconductor, has been reported to be between 1.4 and 1.6 eV [2,4,7,16,18]. It can be said that the estimated results are quite close to the optimum band gap for a solar cell. Fig. 7

As it is generally known that, additives used in aqueous methods control the surface morphology, crystalline structure, grain size, internal stress, corrosion behavior, and even chemical composition [60,61]. In sol–gel method, sol stabilization which has been usually made by using DEA is one of the essential steps in the film formation [43]. In precursor preparing step, DEA content deeply affects the solution properties such as density, color, amount of dissolved substances, and homogeneity. As it is discussed in SEM and XRD studies, DEA amount changed the morphology and structure of the films. Thus, the

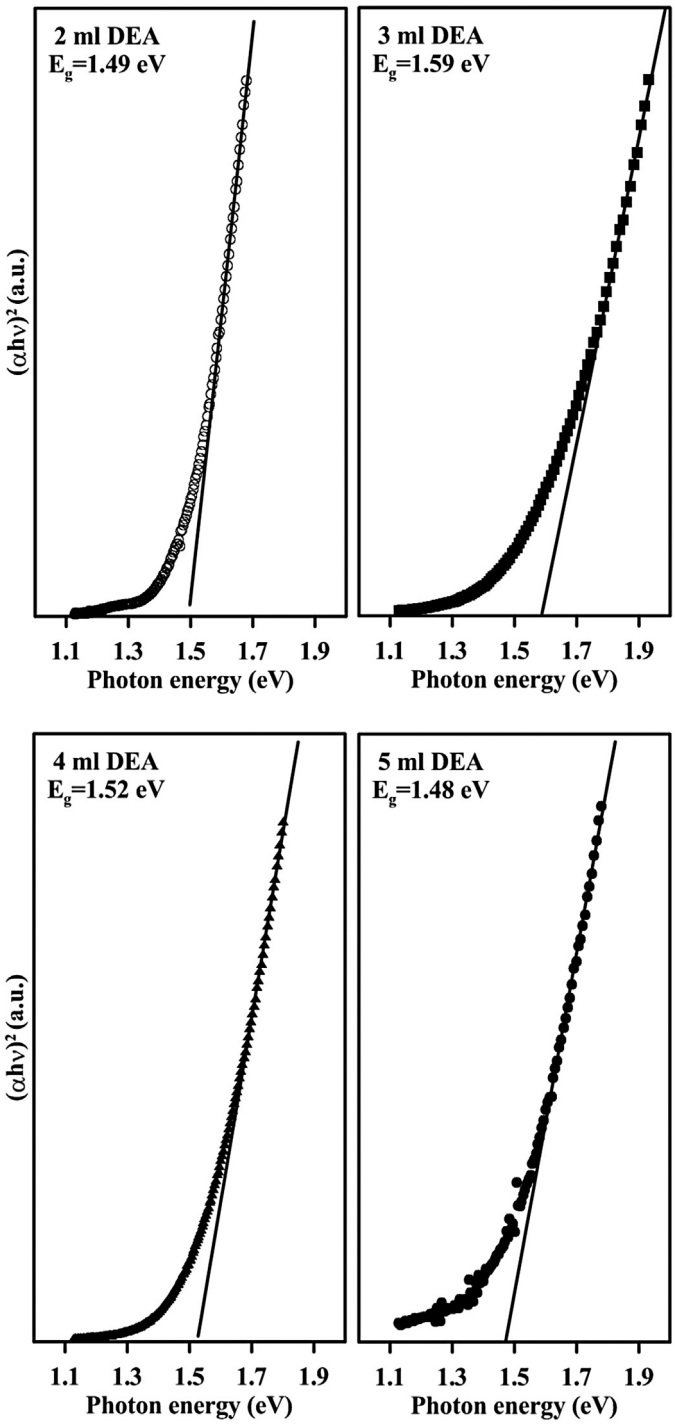

Fig. 7. Band-gap photon-energy estimations of the CZTS films.

variation in the optical band gap values of the samples may be attributed to grain size, morphology, and chemical composition.

4. Conclusions

We prepared high-quality, dense CZTS thin films on quartz-glass and n-type silicon substrates using the sol–gel spin-coating method and investigated the structural, morphological, electrical, and optical properties of CZTS films with respect to DEA content in sol solution. To tolerate sulfur loss during annealing, the annealing process was carried out in a vacuumed quartz tube containing elemental sulfur which is a non-toxic material. The effects of DEA content in the sol solution on the structural, morphological, electrical, and optical properties of the films were investigated in detail. From the XRD results, the diffraction patterns of the samples matched very well with the references and indicated the polycrystalline nature of the films. In the patterns of the samples deposited in the solutions containing 3, 4, and 5 ml DEA, some other peaks indicating the presence of SnS phase were observed. Raman spectroscopy analyses confirmed phase purity of the film produced by using 2 ml of diethanolamine in solution. The crystallite sizes of the films significantly increased with increasing DEA content. DEA content in the growth solution dramatically affected the crystal structure and phase purity of the CZTS films. The plain-view SEM images revealed that the studied samples show smooth, compact, and densely packed morphology. The variations in electrical resistivity and activation energies were attributed to delocalized phonon states generating from the presence of other phases/lattice defects. Under different illumination densities, the n-Si/CZTS junction exhibited good photoconductivity. The I_{on}/I_{off} ratios confirmed the photo-sensitivity of the produced structure. Optical band gap values of the films were estimated via UV–vis spectroscopy and found very quite close to the optimum band gap for a solar cell. In a further study, the effects of smaller DEA contents in CZTS sol solution will be investigated.

Acknowledgements

We would like to thank Assist. Prof. Slavko Bernik and to Ms. Mateja Podlogar for their supports during the study. The financial support from Scientific Research Commission (BAP) of Mustafa Kemal University (Project No: 1204D0102) and Slovenian Research Agency. (Program Contract No. P2-0084-0106/04) are greatly appreciated.

References

[1] S.M. Pawar, B.S. Pawar, A.V. Moholkar, D.S. Choi, J.H. Yun, J.H. Moon, S.S. Kolekar, J.H. Kim, Electrochem. Acta 55 (2010) 4057.
[2] P.K. Sarswat, M. Snure, M.L. Free, A. Tiwari, Thin Solid Films 520 (2012) 1694.
[3] K. Ito, T. Nakazawa, Jpn. J. Appl. Phys. 27 (1988) 2094.
[4] H. Katagiri, K. Jimbo, S. Yamada, T. Kamimura, W.S. Maw, T. Fukano, T. Ito, T. Motohiro, Appl. Phys. Express 1 (2008) 041201.
[5] A. Ennaoui, M. Lux-Steiner, A. Weber, D. Abou-Ras, I. Kotschau, H.-W. Schock, R. Schurr, A. Holzing, S. Jost, R. Hock, T. Vob, J. Schulze, A. Kirbs, Thin Solid Films 517 (2009) 2511–2514.
[6] H. Katagiri, K. Saitoh, T. Washio, H. Shinohara, T. Kurumadani, S. Miyajima, Sol. Energy Mater. Sol. Cells 65 (2001) 141–148.
[7] W. Daranfed, M.S. Aida, N. Attaf, J. Bougdira, H. Rinnert, J. Alloys Compd. 542 (2012) 22–27.
[8] T.K. Todorov, K.B. Reuter, D.B. Mitzi, Adv. Mater. 22 (2010) E156–E159.
[9] W. Shockley, Solid-State Electron. 2 (1961) 35–60.
[10] E. David, Carls on Chief Scientist BP Solar, 14 March 2010, Retrieved 10 February 2011.
[11] K. Wang, O. Gunawan, T. Todorov, B. Shin, S.J. Chey, N.A. Bojarczuk, D. Mitzi, S. Guha, Appl. Phys. Lett. 97 (2010) 143508–143510.
[12] P.A. Fernandes, P.M.P. Salomé, A.F. da Cunha, Thin Solid Films 517 (2009) 2519–2523.
[13] P.A. Fernandes, P.M.P. Salomé, A.F. da Cunha, B.A. Schubert, Thin Solid Films 519 (2011) 7382–7385.
[14] P.A. Fernandes, P.M.P. Salomé, A.F. da Cunha, J. Alloys Compd. 509 (2011) 7600–7606.
[15] H. Katagiri, Thin Solid Films 480–481 (2005) 426–432.
[16] B.A. Schubert, B. Marsen, S. Cinque, T. Unold, R. Klenk, S. Schorr, H.W. Schock, Prog. Photovolt. Res. Appl. 19 (2011) 93–96.
[17] H. Araki, A. Mikaduki, Y. Kubo, T. Sato, K. Jimbo, W.S. Maw, H. Katagiri, M. Yamazaki, K. Oishi, A. Takeuchi, Thin Solid Films 517 (2008) 1457–1460.
[18] J.S. Seol, S.Y. Lee, J.C. Lee, H.D. Nam, K.H. Kim, Sol. Energy Mater. Sol. Cells 75 (2003) 155–162.
[19] T. Yamaguchi, T. Kubo, K. Maeda, S. Niiyama, T. Imanishi, A. Wakahara, Int. Conf. Electrical Eng. (2009).
[20] X. Zhang, X. Shi, W. Ye, C. Ma, C. Wang, Appl. Phys. A: Mater. Sci. Process 94 (2009) 381–386.
[21] J.J. Scragg, P.L. Dale, L.M. Peter, Electrochem. Commun. 10 (2008) 639–642.
[22] J.J. Scragg, D.M. Berg, P.J. Dale, J. Electroanal. Chem. 646 (2010) 52–59.

[23] K. Tanaka, Y. Fukui, N. Moritake, H. Uchiki, Sol. Energy Mater. Sol. Cells 95 (2011) 838–842.
[24] K. Maeda, K. Tanaka, Y. Fukui, H. Uchiki, Sol. Energy Mater. Sol. Cells 95 (2011) 2855–2860.
[25] K. Tanaka, M. Oonuki, N. Moritake, H. Uchiki, Sol. Energy Mater. Sol. Cells 93 (2009) 583–587.
[26] N. Moritake, Y. Fukui, M. Oonuki, K. Tanaka, H. Uchiki, Phys. Status Solidi C 6 (2009) 1233–1236.
[27] P.K. Sarswat, M.L. Free, Phys. Status Solidi (A) 208 (2011) 2861–2864.
[28] A. Fischereder, T. Rath, W. Haas, H. Amenitsch, J. Albering, D. Meischler, S. Larissegger, M. Edler, R. Saf, F. Hofer, G. Trimmel, Chem. Mater. 22 (2010) 3399–3406.
[29] H. Park, Y.H. Hwang, B.S. Bae, J. Sol–Gel Sci. Technol. (2013), http://dx.doi.org/10.1007/s10971-012-2703-0.
[30] K. Tanaka, N. Moritake, H. Uchiki, Sol. Energy Mater. Sol. Cells 91 (2007) 1199–1201.
[31] M.Y. Yeh, C.C. Lee, D.S. Wuu, J. Sol–Gel Sci. Technol. 52 (2009) 65–68.
[32] T.K. Chaudhurin, D. Tiwari, Sol. Energy Mater. Sol. Cells 101 (2012) 46–50.
[33] S.S. Mali, B.M. Patil, C.A. Betty, P.N. Bhosale, Y.W. Oh, S.R. Jadkar, R.S. Devan, Y.R. Ma, P.S. Patil, Electrochim. Acta 66 (2012) 216–221.
[34] Z. Su, C. Yan, K. Sun, Z. Han, F. Liu, J. Liu, Y. Lai, J. Li, Y. Liu, Appl. Surf. Sci. 258 (2012) 7678–7682.
[35] M. Grosberg, J. Krustok, M. Grossberg, J. Krustok, J. Raudoja, T. Raadik, Appl. Phys. Lett. 101 (2012) 102102.
[36] N. Poornima, V.G. Rajeshmon, C. Sudha Kartha, K.P. Vijayakumar, AIP Conf. Proc. 1512 (2013) 464–465.
[37] E. Kask, T. Raadik, M. Grossberg, R. Josepson, J. Krustok, Energy Procedia 10 (2011) 261–265.
[38] O. Gunawan, T. Gokmen, S. Byungha, S. Guha, Photovoltaic Specialists Conference (PVSC), in: 38th IEEE, 2012, 003001-003003.
[39] J.P. Leitao1, N.M. Santos, P.A. Fernandes, P.M.P. Salom, A.F. da Cunha, J.C. Gonzalez, G.M. Ribeiro, F.M. Matinaga, Phys. Rev. B 84 (2011) 024120–024127.
[40] S.W. Shin, S.M. Pawar, C.Y. Park, J.H. Yun, J.H. Moon, J.H. Kim, J.Y. Lee, Sol. Energy Mater. Sol. Cells 95 (2011) 3202–3206.
[41] T. Prabhakar, N. Jampana, Sol. Energy Mater. Sol. Cells 95 (2011) 1001–1004.
[42] S.S. Mali, P.S. Shinde, C.A. Betty, P.N. Bhosale, Y.W. Oh, P.S. Patil, J. Phys. Chem. Solids 73 (2012) 735–740.
[43] R.C. Kaminski, S.H. Pulcinelli, A.F. Craievich, C.V. Santilli, J. Eur. Ceram. Soc. 25 (2005) 2175–2180.
[44] Y. Djoued, R. Taj, R. Bruning, S. Badilescu, P.V. Ashrit, G. Bader, T.V. Van, J. Noncryst, Solids 297 (2002) 55–66.
[45] P. Zhang, J. Yuan, C. Hao, Powder Technol. 195 (2009) 166–170.
[46] K. Murugan, N.R. Tata, G.V. Narashima Rao, S. Ashutosh Gandhi, B.S. Murty, Mater. Chem. Phycs. 129 (2011) 810–815.
[47] H.J. Chen, L. Wang, W.-Y. Chiu, Mater. Chem. Phys. 101 (2007) 12–19.
[48] Y. Djaoude, M. Thibodeau, J. Robichand, S. Balaji, S. Prya, N. Tchoukanova, S.S. Bates, J. Photchem. Photobiol. A: Chem. 193 (2008) 271–283.
[49] J. Yu, M. Zhou, H. Yu, Q. Zhang, Y. Yu, Mater. Chem. Phys. 95 (2006) 193–196.
[50] H.S. Jung, J.K. Lee, J.Y. Kim, K.S. Hong, J. Solid State Chem. 175 (2003) 278–283.
[51] C. Sanchez, J. Livage, M. Henry, F. Babonneau, J. Non-Cryst. Solids 100 (1988) 65–76.
[52] Y. Takahashi, A. Ohsugi, T. Arafuka, T. Ohya, T. Ban, Y. Ohya, Sol–gel Sci. Technol. 17 (2000) 224–238.
[53] Y. Takahashi, Y.J. Matsuoka, J. Mater. Sci. 23 (1988) 2259–2266.
[54] Y. Takahashi, K. Yamacuchi, J. Mater. Sci. 25 (1990) 3950–3955.
[55] Y. Ohya, H. Saiki, Y. Takahashi, J. Mater. Sci. 29 (1994) 4099–4103.
[56] G. Knuyt, C. Quaeyhaegens, J.D. Haen, L.M. Stals, Phys. Status Solidi B 195 (1996) 179–193.
[57] Rruff open Raman database, ID: R120098.2, rruff.info/kesterite/desc/R120098.
[58] J. Owens, L. Gladczuk, R. Szymczak, P. Dluzewski, A. Wisniewski, H. Szymczak, A. Golnik, C. Bernhard, C. Niedermayer, High temperature magnetic order in zinc sulfide doped with copper, J. Phys. Chem. Solids 72 (2011) 648–652.
[59] J. Tauc, Mater. Res. Bull. 5 (1970) 721–730.
[60] M. Mouanga, L. Ricq, G. Douglade, J. Douglade, P. Berçot, Surf. Coat. Technol. 201 (2006) 762.
[61] M. Mouanga, L. Ricq, L. Ismaili, B. Refouvelet, P. Berçot, Surf. Coat. Technol. 201 (2007) 7143.